Atmos. Chem. Phys. Discuss., 11, 11455–11495, 2011
www.atmos-chem-phys-discuss.net/11/11455/2011/
doi:10.5194/acpd-11-11455-2011

Atmospheric Chemistry and Physics Discussions

Using boundary layer equilibrium to reduce uncertainties in transport models and CO_2 flux inversions

I. N. Williams[1], W. J. Riley[2], M. S. Torn[2], J. A. Berry[3], and S. C. Biraud[2]

[1]Department of Geophysical Sciences, University of Chicago, Chicago, IL, USA
[2]Lawrence Berkeley National Laboratory, Earth Sciences Division, Berkeley, CA, USA
[3]Carnegie Institution of Washington, Stanford, CA, USA

Received: 18 February 2011 – Accepted: 30 March 2011 – Published: 13 April 2011

Correspondence to: I. N. Williams (inw@uchicago.edu)

Published by Copernicus Publications on behalf of the European Geosciences Union.

Abstract

This paper reexamines evidence for previously hypothesized errors in atmospheric transport models and CO_2 flux inversions by evaluating the diagnostics used to infer vertical mixing rates from observations. Several conventional mixing diagnostics are compared to analyzed mixing using data from the US Southern Great Plains Atmospheric Radiation Measurement Climate Research Facility, the CarbonTracker data assimilation system based on Transport Model version 5 (TM5), and atmospheric reanalyses. The results demonstrate that previous diagnostics based on boundary layer depth and vertical concentration gradients are unreliable indicators of vertical mixing. Vertical mixing rates are anti-correlated with boundary layer depth at some sites, diminishing in summer when the boundary layer is deepest. Vertical CO_2 gradients between the boundary layer and free-troposphere are strongly affected by seasonal surface fluxes and therefore do not accurately reflect vertical mixing rates. The finite timescale over which vertical tracer gradients relax toward equilibrium is proposed as an improved mixing diagnostic, which can be applied to observations and model simulations of CO_2 or other conserved boundary layer tracers with surface sources and sinks. This diagnostic does not require dynamical variables from the transport models, and is independent of possible systematic biases in prior- and post-inversion seasonal surface fluxes. Results indicate that observations frequently cited as evidence for systematic biases in atmospheric transport models are insufficient to prove that such biases exist. Some previously hypothesized transport model biases, if found and corrected, could cause inverse estimates to further diverge from land-based estimates.

1 Introduction

Coupled carbon-climate models predict that the fraction of anthropogenic CO_2 emissions absorbed by ecosystems will decrease over the 21st century (Friedlingstein et al., 2006; Denman et al., 2007), but how accurately these models represent current

ACPD
11, 11455–11495, 2011

ecosystem CO_2 sources and sinks is unclear. The present-day partitioning between tropical and mid-latitude ecosystem sources and sinks is itself unknown due to uncertainties in the contribution of atmospheric mixing and transport to observed CO_2 concentrations (Bousquet et al., 2000; Peylin et al., 2002; Rodenbeck et al., 2003; Baker et al., 2006; Stephens et al., 2007). Reducing these uncertainties is a major challenge in assessing the net impact of anthropogenic emissions on global climate.

Uncertainty in the global distribution of ecosystem CO_2 sources and sinks has been attributed to errors in the transport models used for CO_2 inversions (Fung et al., 1983; Denning et al., 1995; Gloor et al., 1999; Dargaville et al., 2003; Baker et al., 2006; Yang et al., 2007; Stephens et al., 2007), yet the problem of identifying these errors remains. Net ecosystem exchange varies seasonally over mid-latitudes but corresponding spatial concentration gradients are weaker in summer when CO_2 uptake coincides with stronger atmospheric mixing and transport. This covariance between atmospheric dynamics and ecosystem exchange, known as the atmospheric rectifier effect, produces enhanced annual-mean near-surface concentrations relative to the overlying atmosphere even over annually-balanced ecosystems (Fung et al., 1983; Denning et al., 1995, 2008).

Conventional wisdom is that the depth of boundary layer mixing plays the dominant role in the rectifier effect, since solar forcing drives both boundary layer mixing and ecosystem exchanges. Analyses of field measurements have shown that the dilution of concentrations by boundary layer depth variations is of comparable magnitude to net ecosystem exchange over the diurnal cycle (Raupach, 1991; Raupach et al., 1992; Levy et al., 1999; Lloyd et al., 2001; Styles et al., 2002), suggesting that boundary layer depth is a key indicator of mixing strength. Atmospheric transport models are known to underestimate summer boundary layer depths, which could lead to underestimation of inferred northern terrestrial CO_2 sinks and further increase the discrepancy between atmospheric inverse and carbon inventory estimates of the global carbon budget (Denning et al., 1995; Chen et al., 2004; Yi et al., 2004; Yang et al., 2007; Denning et al., 2008). However, systematic differences between transport model

ACPD
11, 11455–11495, 2011

simulations and observed vertical CO_2 profiles are more consistent with overestimated mixing, implying that the strength of northern terrestrial CO_2 sinks is overestimated in the inversions and could be reconciled with carbon inventories if transport models were improved (Stephens et al., 2007).

Our objective is to unify these studies by reexamining the evidence for transport model errors in terms of the mechanisms producing observed CO_2 gradients. We will demonstrate that the lower-tropospheric CO_2 budget is strongly timescale dependent, so that the transport and mixing derived from any one field study is relevant only in the context of the timescale over which the measurements were taken or analyzed. We use this timescale dependence to develop an equilibrium boundary layer model for vertical CO_2 gradients and to develop a new diagnostic of transport and mixing that can be applied to transport model simulations and observations at seasonal and longer timescales. We will show that the equilibrium boundary layer model serves as a useful test of hypotheses proposed to reconcile atmospheric CO_2 inversions with carbon inventory estimates of global carbon sinks.

2 Physical basis

2.1 Mixed-layer approximation

Atmospheric transport and mixing cannot be observed directly, so it is necessary to consider simplified tracer conservation equations to interpret differences between models and observations. A common simplifying assumption is based on the observation that dry convective mixing is sufficiently fast to maintain well-mixed trace gases (CO_2) in the boundary layer (Emanuel, 1994). The boundary layer satisfying this well-mixed assumption is hereafter referred to as the mixed-layer. The mixed-layer tracer conservation equation in the absence of horizontal advection (considered in Sect. 4.3) and

ACPD
11, 11455–11495, 2011

cloud fluxes can be written as

$$\rho_m \partial_t (h c_m) - \rho_f c_f \partial_t h + \rho_f w (c_f - c_m) = F \quad (1)$$

where Reynolds averaging is implied; h is the mixed-layer height; c_f and c_m are the free troposphere and mixed-layer mixing ratios, respectively; ρ is atmospheric molar density; w is the vertical wind velocity evaluated at the mixed layer height; and subscripts f and m denote quantities at the free-troposphere level just above the mixed-layer and averaged within the mixed layer, respectively. The surface flux (F) in Eq. (1) is the net ecosystem exchange, and balances the sum of CO_2 storage in the mixed-layer and entrainment of free-troposphere CO_2 owing to growth of the mixed-layer into the free-troposphere (sum of the first two left-hand side terms), as well as vertical advective transport averaged over the mixed-layer (third LHS terms). Note that there is no contribution to the vertical advective tendency by vertical motion exceeding the growth rate of the mixed-layer, since net loss of mixed-layer air to the free-troposphere changes only the volume of the mixed-layer and not the mixed-layer concentration. Horizontal advection may be significant in these cases and is considered in later sections.

The mixed-layer approximation (Eq. 1) is not strictly valid at night, when turbulence becomes shallow and surface emissions (e.g., ecosystem respiration) accumulate in the shallow nocturnal boundary layer. However the rapid decay of turbulence after sunset leaves a relic mixed-layer, or so-called residual layer, extending from the nocturnal boundary layer to the depth of the afternoon mixed-layer, in which CO_2 concentrations are similar to the afternoon mixed-layer (Yi et al., 2001). Since h is a limit of integration in the derivation of Eq. (1), it can be taken without additional approximation to be the total depth of the residual-layer and mixed-layer system. Equation (1) can be integrated over the diurnal cycle by assuming (1) that depth-integrated advective tendencies (the third term of Eq. 1) are much larger in the residual layer than the nocturnal boundary layer, due to the much larger residual layer depth and wind speed; and (2) that the nighttime vertical concentration gradient between free-troposphere and residual layer is steady and given by the daytime or afternoon concentration gradient. Since CO_2 is

ACPD
11, 11455–11495, 2011

conserved, any CO_2 that accumulates in the shallow nocturnal boundary layer is accounted for by the daytime mixed-layer concentration. These approximations, which we apply here, have been used in various forms to close the CO_2 budget over diurnal cycles (Chou et al., 2002; Bakwin et al., 2004; Helliker et al., 2004; Yi et al., 2004).

2.2 Scaling

Further approximations to Eq. (1) have been made by neglecting either entrainment and storage (Bakwin et al., 2004; Helliker et al., 2004) or vertical advection (e.g. Yi et al., 2004), referred to here as the equilibrium and non-equilibrium approximations, respectively. The choice of approximation is crucial to the interpretation of observations and transport model errors. To inform the appropriate approximation, we apply dimensional analysis to Eq. (1). The ratio of the sum of CO_2 storage and entrainment to vertical advection is scaled according to the ratio of a mixed-layer relaxation time (τ) to a characteristic timescale (T) of Eq. (1). The mixed-layer relaxation time is given by the ratio of characteristic mixed-layer depth to vertical velocity ($\tau = H/W$). The timescale (T) is determined by averaging Eq. (1) over time. We will refer to the ratio of these timescales as t^* ($t^* = H/WT$). Although both equilibrium and non-equilibrium approximations have been used to interpret seasonal variability in atmospheric CO_2, equilibrium assumes that the seasonal cycle is long compared to the mixed-layer relaxation time (i.e. $t^* \ll 1$) whereas non-equilibrium assumes that this ratio is large ($t^* \gg 1$). Dimensional analysis therefore predicts that the equilibrium assumption becomes increasingly valid at longer timescales and for stronger atmospheric circulations. We will test these predictions in the following section.

ACPD
11, 11455–11495, 2011

3 Observational evidence

3.1 Study site

We tested the hypothesis that the CO_2 budget is a function of the timescale over which it is observed using atmospheric concentration measurements collected at the Central Facility (36.61° N, 97.49° W) of the US Southern Great Plains Atmospheric Radiation Measurement Climate Research Facility (SGP) between January 2003 and January 2008. More than 80% of the land surface of the Southern Great Plains is managed for agriculture and grazing (Fischer et al., 2007). Winter wheat grows from November through June over 40% of the region (Fischer et al., 2007), mostly to the southeast (Riley et al., 2009), with the remaining area dominated by pasture (40%) and a mixture of C_3 and C_4 crops (20%) that grow from April through August (Cooley et al., 2005).

3.2 Timeseries

A precision gas system (Bakwin et al., 1995) was used to obtain mixed-layer CO_2 concentrations at 15 min intervals on the 60 m tower. Pressurized air samples have been collected approximately weekly on the 60 m tower and in the free-troposphere at SGP for subsequent analysis at NOAA/ESRL. The continuous mixed-layer CO_2 concentrations were compared with the flask-based measurements to account for and correct possible drifts. These flask-based measurements include, but are not limited to, CO_2, CH_4, CO, N_2O, CO, SF_6, H_2, and ^{13}C and ^{18}O in CO_2. The sample collection procedures have been described in detail in Conway et al. (1994). Typically, air was pumped into a pair of 2.5 L glass flasks, connected in series, and slightly pressurized above ambient pressure. Analyses to follow required free-troposphere mixing ratios just above the mixed-layer (Fig. 1b), which were obtained from the first available flask sample just above the CT/TM5 mixed-layer depth (typically available at altitudes of 457.2, 609.6, 914, 1219.2, 1524, 1828.8, 2133.6, 2438.4, and 2743.2 m above ground, and higher, with an uncertainty of about 30 m).

ACPD
11, 11455–11495, 2011

The timeseries of mixed-layer CO_2 concentrations (Fig. 1) provides evidence that analyses of short-term field observations cannot be extrapolated to explain the seasonal rectifier effect. As the averaging time increases the growth and decay of mixed-layer concentrations does not correspondingly increase, as seen by comparing the 1 day and 90 day running averages of mixed-layer CO_2 in Fig. 1a. Therefore we conclude that the magnitude of mixed-layer CO_2 storage decreases when the length of the running averages increases. Similar results have been obtained previously (Davis et al., 2003) based on observations at a tall-tower in Wisconsin (hereafter LEF). The magnitude of mixed-layer depth variations also does not increase between daily and seasonal timescales (Fig. 1c), suggesting that the importance of entrainment to the seasonal rectifier effect may also be overemphasized if analyses of the CO_2 budget are extrapolated from daily or synoptic timescales to the seasonal cycle. These conclusions are made more quantitative in the following.

3.3 Calculation of budget terms

Entrainment and storage were analyzed according to Eq. (1) from day-to-day changes in afternoon (01:00–04:00 p.m. LT), as described in Sect. 2.1. Mixed-layer depths were obtained from the CarbonTracker data assimilation system (hereafter CT/TM5). CT/TM5 combines CO_2 surface exchange models and a global, two-way nested atmospheric transport model driven by meteorological fields from the European Centre for Medium-Range Weather Forecasts (ECMWF). Mixed-layer depth and the three-dimensional distribution of CO_2 mole fractions and surface fluxes were available at $1^\circ \times 1^\circ$ spatial resolution every 3 h.

Vertical advection was not archived in the 2008 CT/TM5 dataset, and was recreated here with vertical velocities from the ECMWF interim reanalysis (Fig. 1d), based on the same general circulation model and parameterization schemes in CT/TM5 (Peters et al., 2007). Differences between our recreated advective tendencies and CT/TM5 are expected in part due to differences in the forecast time-steps used to create each dataset, and interpolation of the ECMWF meteorological data from $1.5^\circ \times 1.5^\circ$ to $1^\circ \times 1^\circ$

ACPD
11, 11455–11495, 2011

resolution in CT/TM5. We averaged the two CT/TM5 grid-points closest to each of our study sites for use with the ECMWF reanalysis vertical velocities, due to the difference in resolution of these products. Additional spatial averaging had little effect on the results. Resolution sensitivity of the recreated vertical advective tendency was investigated by spatially averaging ECMWF velocities over the 1 through 4 grid-cells nearest the SGP site, and was found to be small. Sensitivity was further tested using vertical velocities from three independent data assimilation systems (RUC, NCEP, and NARR), which were qualitatively similar to ECMWF velocities and did not have a notable effect on our results.

3.4 Timescale dependence

Observations from the SGP tower and assimilated data from CT/TM5 were used to quantify the timescale dependence of lower-tropospheric CO_2. The timeseries for each budget term in Eq. (1) was divided into non-overlapping segments of length ranging from 1 to 90 days, and each budget term was averaged over each of these segments (storage and entrainment were added together to form a single budget term). This procedure resulted in a statistical ensemble of CO_2 budgets, with one ensemble for each of the averaging times ranging from 1 to 90 days. After taking the magnitude of each term, we calculated the ensemble-median of the ratios of terms.

The ratios of budget terms (Fig. 2) confirm that the relative importance of entrainment and storage is a strong function of timescale at the three sites tested, with entrainment and storage becoming an order of magnitude smaller than surface fluxes by monthly and longer timescales. These results are based on surface fluxes from the CT/TM5 data assimilation system and entrainment and storage calculated using mixing ratios from the same dataset. The three test sites are SGP, described in the section above; LEF (45.95° N, 90.27° W), characterized by a managed forest of mixed northern hardwood, aspen, and wetlands; and Harvard Forest (HFM, 42.54° N, 72.17° W), a managed, deciduous forest, and were chosen to correspond to the North American aircraft flask sampling locations used in a related study (Stephens et al., 2007). Coastal and

ACPD
11, 11455–11495, 2011

mountainous sites (EFM and CAR in Stephens et al., 2007) were excluded from our analysis because the calculation of vertical advection may be influenced by differences in model topography and resolution between CT/TM5 and the ECMWF interim reanalysis. The CT/TM5 concentrations used here were vertically averaged over the mixed layer to define the mixed-layer concentrations.

The results (Fig. 2) indicate a general timescale dependence of the CO_2 budget for continental mixed-layers. The comparison confirms that entrainment and storage are of secondary importance relative to both advective transports and surface fluxes at seasonal timescales. The results hold for budget terms calculated using mixing ratios from CT/TM5 (Fig. 3b) and from tower and aircraft observations (Fig. 3a).

3.5 Scaling relationship for mixed-layer tracer budgets

Advection and net surface flux dominate the budget of mixed-layer CO_2 at seasonal timescales, but at a rate which varies quantitatively between sites in North America and between seasons (Fig. 3b). The scaling relationship developed in Sect. 2.1 predicts that mixed-layer budgets depend not only on the averaging time, but on the ratio of the averaging time to the boundary layer relaxation time, which depends on the strength of the local circulation. To test this hypothesis we reproduced the results of Fig. 3a,b in a scatter plot where each point represents the sum of entrainment and storage (y-axis), and advection (x-axis), corresponding to a given averaging time (Fig. 4a,d). The scatter plots were made by binning the results of the ensemble budget (shown in Fig. 3) into 10 bins according to averaging time, where the bin spacing is allowed to be uneven so that there are equal numbers of ensemble members in each bin. The same timescale dependence shown in Fig. 3 is recovered in Fig. 4a,d except the scatter plots reveal the individual magnitudes of entrainment and storage, and advection, and their standard deviations (numbered labels in Fig. 4a,d represent mean averaging times for each bin).

The differences between mixed-layer budgets at different timescales and continental locations can be understood in terms of the averaging time and the strength of the local circulation. To demonstrate this relationship we scaled the vertical advection

ACPD
11, 11455–11495, 2011

term by the non-dimensional number t_0^* (Sect. 2.2), calculated with mixed layer depths and vertical velocities (H_0, W_0) averaged across the three sites (SGP, LEF, HFM). The budget terms were binned again using t_0^* as opposed to the averaging time. Typical values of t_0^* (and t^*) range from 1.5 to 0.01 for averaging times of 1 day to 90 days, respectively. The results (Fig. 4b,e) confirm that the ratio of entrainment plus storage to advection scales linearly with t_0. Differences in the slopes of the linear relations, particularly between HFM and the other two sites, are eliminated when further scaled according to t^*, where the contribution of differences in local atmospheric circulation is taken into account (Fig. 4c,f) by calculating mixed layer depths and vertical velocities at each site.

We conclude that the mechanisms found to control tracer vertical gradients over the course of a field campaign could vary considerably from the mechanisms operating over longer timescales and at different locations. Storage and entrainment are relatively large components of the atmospheric CO_2 budget over the diurnal cycle, and are proportional to mixed-layer depth variations, so that mixed-layer depth variations explain a large portion of the mixing between the free-troposphere and boundary layer at the daily timescale. However this mixing is controlled by the vertical advective transport at longer timescales, which does not necessarily scale with mixed-layer depth. The following sections develop a new diagnostic of vertical mixing valid at seasonal timescales.

4 Boundary layer quasi-equilibrium

4.1 Theoretical basis

We have shown that mixed-layer depth is not a reliable indicator of mixing strength when t^* is small, typically at seasonal timescales. In this limit the tracer conservation Eq. (1) yields a balance between vertical advective transport and net surface flux. Here we explore the finite timescale over which equilibrium is approached, and whether this

ACPD
11, 11455–11495, 2011

timescale is diagnostic of mixing rates. For example, consider the assumption that free-troposphere mixing ratios vary slowly in time compared to mixed layer mixing ratios. Equation (1) can then be written as

$$\rho \frac{d}{dt}(h\Delta c) + \rho \langle \partial_x u \rangle h \Delta c = F\,, \tag{2}$$

where Δc is the difference in mixing ratio ($c_m - c_f$) between the free troposphere and mixed layer, and vertical velocity has been rewritten in terms of the vertically integrated horizontal divergence (bracketed term in Eq. 2) using the continuity equation (the horizontal wind velocity, u, is written entirely in the x-direction for brevity). If horizontal wind divergence and surface flux are slowly varying in time compared to perturbations in the mixed-layer depth and vertical mixing ratio difference, we obtain a solution

$$h\Delta c = \left[(h\Delta c)_{t_0} - F\langle \partial_x u \rangle^{-1}\right] \exp(-\langle \partial_x u \rangle t) + F\langle \partial_x u \rangle^{-1}\,. \tag{3}$$

Equation (3) predicts that tracer vertical gradients relax toward equilibrium at a rate determined by the rate of mass divergence in the mixed-layer. Horizontal advection and non-linear vertical tracer advection have been neglected, however the slowly varying components of these terms can be considered part of the steady forcing (i.e., can be combined with the surface flux, F) without changing the predicted exponential decay of perturbations. This solution compares favorably to observational data, shown in the following section.

In the long-time limit ($t \gg \langle \partial_x u \rangle^{-1}$) we obtain the equilibrium solution given by $h\Delta c \approx F\langle \partial_x u \rangle^{-1}$. The weighting of the vertical gradient (Δc) by h reflects the fact that the divergent circulation transports more mixed-layer mass per surface area as the depth of the mixed-layer increases, requiring either larger surface flux or smaller tracer vertical gradients to balance tracer transport. Although fluctuations in h can still produce fluctuations in Δc at any given time, a statistically steady state is expected when the relaxation time (given by $\langle \partial_x u \rangle^{-1}$) is short compared to the averaging time. In this limit we obtain the equation in Bakwin et al. (2004) and Helliker et al. (2004),

$$-\overline{w}(\overline{c_m} - \overline{c_f}) = F \tag{4}$$

ACPD
11, 11455–11495, 2011

where the continuity equation has been used to write the average divergence in terms of the average vertical velocity, and over-bars represent time-averaging (e.g., 90 day seasonal averages), and F is understood to be the slowly varying (seasonal) component of surface flux. The solution (Eq. 3) is consistent with our earlier scaling arguments (Sect. 2.2), which predicted a balance between advective tracer transport and surface fluxes for long averaging times relative to the relaxation time (i.e. $t^* \ll 1$). This quasi-equilibrium solution (Eq. 4) is analogous to that of boundary layer entropy or convective-available potential energy in the quasi-equilibrium theory for tropical climate (Raymond, 1997). Equation (4) illustrates why systematic errors in vertical concentration gradients among transport models do not necessarily reflect systematic errors in modeled transport or mixing, since Δc is also affected by possible systematic errors in the surface flux (F).

4.2 Relaxation times

Vertical CO_2 gradients, when taken alone, are poor indicators of lower-tropospheric mixing and transport because of the presence of strong surface fluxes, as shown by Eq. (4) and the scaling arguments of Sect. 2.2. Since we are interested in evaluating the mixing and transport properties of models, we wish to separate the influence of surface fluxes from that of mixing in a diagnostic model. Here we demonstrate that the relaxation timescale is suitable for this purpose. Differences in relaxation times can be understood through Eq. (3) in terms of the modeled divergent wind, which could reflect errors in parameterized turbulent mass flux, resolved advection, or parameterized moist convection in transport models (as discussed in Sect. 1). The results will also support the equilibrium approximation (Eq. 4) by demonstrating that relaxation times are generally much shorter than the seasonal timescale and shorter than the synoptic timescale.

We compared the observed relaxation time to that predicted by Eq. (3) by comparing the autocorrelation of observed fluctuations in the vertical CO_2 gradient to that predicted by Eq. (3). Equation (2) can be written in terms of fluctuations about an

ACPD
11, 11455–11495, 2011

ensemble average by substituting the quasi-equilibrium solution (Eq. 4) for the average vertical concentration gradient (i.e. $F\langle\partial_x u\rangle^{-1} \approx \overline{h}\,\overline{\Delta c}$) and subtracting $\langle\partial_x u\rangle\overline{h}\,\overline{\Delta c}$ from Eq. (2) to yield,

$$\frac{d}{dt}C + \langle\partial_x u\rangle C = 0 \tag{5}$$

where C is the fluctuation given by $h\Delta c - \overline{h}\,\overline{\Delta c}$, and density is assumed constant over the relaxation timescale. The autocorrelation function is the exponential decay given by

$$\frac{\overline{C(t')C(t)}}{\overline{C^2}} = \exp(-\langle\partial_x u\rangle|t - t'|) \tag{6}$$

where $|t - t'|$ is the time lag of the autocorrelation (e.g. Chatfield, 2004). The derivation is strictly for autocorrelations of fluctuations in $h\Delta c$, but the autocorrelations of Δc were nearly identical in all the cases examined here. Adding fluctuations (F') about the mean surface flux to the right hand side of Eq. (5) yields the familiar Langevin equation (see North et al., 1993, for an analogous application to climate sensitivity), which has the same autocorrelation function (Eq. 6) as long as the fluctuations have the statistical properties of Gaussian white noise. Although the latter assumption is not strictly valid for surface CO_2 fluxes, the solution (Eq. 6) proves to be a useful quantitative description of observed concentration autocorrelations.

A comparison of observed (SGP) and theoretical autocorrelations is shown in Fig. 5, where winter (December–February) and summer (June–August) are shown separately in panels Fig. 5a and Fig. 5b, respectively. Observed vertical gradients were calculated from the difference in mixing ratios between the 60 m tower and aircraft flask samples at SGP. The gray lines in Fig. 5 indicate the theoretical exponential decay calculated from the ECMWF reanalysis divergent wind field (i.e., using Eq. 6, with the full horizontal divergence $\langle\partial_x u + \partial_y v\rangle$). The results confirm the theoretical prediction that

ACPD
11, 11455–11495, 2011

vertical mixing ratio gradients approach a time-mean value approximately exponentially, at a rate determined by the rate of mass divergence in the mixed-layer. Although the quasi-equilibrium theory is based on linear assumptions (i.e. covariation of w and Δc is neglected), the exponential decay of autocorrelations still holds if the non-linear component of advection is slowly varying relative to the relaxation time. Relaxation times were generally less than 3 days, or shorter than the typical synoptic timescale and much shorter than the seasonal timescale.

The above comparison was repeated for the CT/TM5 dataset at SGP, LEF, and HFM. The difference between the summer and winter relaxation times at SGP and HFM is captured by the theoretical solution to the conservation equation (gray lines in Fig. 6), but the summer CT/TM5 concentration gradient at HFM decays faster than theory predicts (Fig. 6c). Note that the theoretical gray lines for SGP in Fig. 5a,b are the same as those in Fig. 6a,d, except for the addition of two years (2001, 2002) of data from the CT/TM5 analyses. Removing the additional two years had no effect on the agreement between observations, theory, and CT/TM5, seen by comparing panels Fig. 5a,b, and Fig 6a,d. Based on this comparison we conclude that there is no evidence for errors in the divergent wind field of the CT/TM5 data assimilation system at SGP. The disagreement between theory and CT/TM5 in summer at HFM (and in winter at LEF) did not improve upon changing the averaging time from 90 to 45 days or 180 days. These results warrant future investigations using data from the measurement towers at LEF and HFM.

Our results show that the rate at which CO_2 vertical gradients relax toward equilibrium can be used to obtain a more reliable mixing diagnostic than using CO_2 vertical gradients alone. One drawback to this method is the requirement that surface fluxes be steady or have the statistical properties of Gaussian white noise on timescales shorter than the relaxation timescale. This assumption also applies to the horizontal advection and cloud mass fluxes included in the more general form of the flux (F) in Eq. (3). The analysis described here could be further tested in future studies using other conserved tracers whose surface fluxes are less likely to be correlated at these short timescales.

ACPD
11, 11455–11495, 2011

Autocorrelations using SF_6 were reported (Denning et al., 1999) and were similar to our results using CO_2, but were not interpreted in terms of the divergent wind field. Our results provide a theoretical basis for relating the autocorrelation to transport statistics from atmospheric models.

4.3 Application to surface fluxes

The equilibrium approximation was further tested by extending Eq. (4) to include horizontal advection and comparing the equilibrium surface fluxes to surface fluxes from the CT/TM5 data assimilation system. Horizontal winds were interpolated to the SGP site, using the interpolation scheme internal to CT/TM5, and gradients were taken from the CT/TM5 data assimilation system. The full non-linear horizontal advection was calculated (i.e., gradients and winds were multiplied before seasonal averaging). We also tested the linearity assumption made in deriving the equilibrium solution (Eq. 4) by calculating the full non-linear vertical advection and dividing this term into linear and nonlinear components following standard Reynolds decomposition, based on 90 day averages (e.g., $w = \overline{w} + w'$, $\Delta c = \Delta\overline{c} + \Delta c'$, where primes denote departure from the 90 day average). A 90 day running average was then taken to write the vertical advection term as the sum of a linear and nonlinear component (i.e., $\overline{w}\Delta\overline{c} + \overline{w'\Delta c'}$).

The full mixed-layer CO_2 budget at SGP is shown in Fig. 7 and is decomposed into the sum of storage and entrainment, vertical advection, and horizontal advection. The CO_2 budget was also calculated using CT/TM5 data for SGP, LEF and HFM (Fig. 8). The total vertical advection (sum of linear and non-linear terms) and the non-linear term are each shown separately in Fig. 8. Vertical advection is typically the dominant term at SGP. The non-linear advection is also significant, at times accounting for most of the vertical advective transport, and highlights the importance of transport by synoptic-scale disturbances. Horizontal advection is smaller than vertical advection but is of the same order of magnitude, whereas storage and entrainment are typically an order of magnitude smaller at seasonal timescales. Net surface fluxes inferred from the mixed-layer budget method are in good agreement with surface fluxes predicted by the

ACPD
11, 11455–11495, 2011

CT/TM5 analyses, as shown in Fig. 9. We extended the mixed-layer approximation to diagnose vertical concentration gradients, as discussed in the following.

4.4 Application to vertical concentration gradients

Previous studies assumed that the mixed-layer acts as a mixing chamber in which concentrations of gases exchanged at the surface are either diluted or concentrated through deep summer or shallow winter mixed layer depths. Studies based on these analogies have emphasized the role of mixed-layer depth in explaining differences between observed and simulated vertical CO_2 gradients between the mixed-layer and the free-troposphere above. Having shown that the analogy to a mixing chamber breaks down at long timescales, we instead hypothesize that vertical concentration gradients come into equilibrium with transport into and out of the mixed-layer and ecosystem exchanges at seasonal timescales.

We used the equilibrium approximation to Eq. (1), including horizontal advection, with vertical advection divided into linear and non-linear components (as in Sect. 4.3), and inverted the slowly-varying component of vertical advective transport to obtain the vertical concentration gradient (here given by $\Delta\overline{c} = \overline{c_m} - \overline{c_f}$), according to

$$\overline{\Delta c} = -\left(F + \overline{w'\Delta c'} - \overline{u\partial_x c_m} - \overline{v\partial_y c_m}\right)/\overline{w} \quad (7)$$

where the last two RHS terms are the zonal and horizontal advection, respectively. Vertical concentration gradients between the free-troposphere and mixed-layer were calculated by applying Eq. (7) to CO_2 concentrations and surface fluxes from CT/TM5. Density differences between the free-troposphere and mixed layer account for less than 10% of the variation in concentration gradients and have been neglected in Eq. (7) to simplify our discussion, but were included in all our computations.

The resulting equilibrium CO_2 vertical gradients (Fig. 10a) at all three sites (SGP, LEF, HFM) compared favorably with those obtained directly from CT/TM5 (Fig. 10b), although there are differences in the magnitude of the seasonal cycle in some years. We did not compare panels (Fig. 10a,b) directly because the differences between CT/TM5

ACPD
11, 11455–11495, 2011

and the equilibrium approximation were within the sensitivity of our results to increasing or decreasing the mixed-layer depth by one vertical model level. Rather we point out that the equilibrium approximation is successful in predicting the seasonal cycle and the differences in annual mean vertical gradient between the three sites. The CO_2 transport considered in this diagnostic is that by the subsiding vertical wind, which is in approximate equilibrium with mixed-layer entrainment of free-tropospheric CO_2. This diagnostic contrasts with previous diagnostics of vertical concentration gradients, which considered transient changes in day-to-day mixed-layer depth as the dominant mechanism of exchange between the free-troposphere and mixed-layer. The latter diagnostic is based on the common assumption that seasonal variations in mixed-layer depth drive annual-mean vertical CO_2 gradients. This assumption is tested in the following section.

4.5 Application to the seasonal rectifier effect

Annual-mean vertical CO_2 gradients result in part from the covariation of atmospheric dynamics with net ecosystem exchanges over the seasonal cycle, known as the vertical rectifier effect, which is frequently attributed to seasonal variation of mixed-layer depths. Mixed-layer depth variations do not explicitly appear in the equilibrium description of vertical concentration gradients (Eq. 7) because, as discussed previously, their direct effect on the dilution of concentrations is an order of magnitude smaller than transport at seasonal timescales. Therefore, we investigate the possibility that seasonally varying transport could explain the rectifier effect. Composite seasonal cycles were calculated by further averaging the 90 day running average subsidence velocities (i.e., the solid black line in Fig. 1d) over the seven annual timeseries extending from 1 January–31 December, for the years that CT/TM5 data were available (January 2001–2008).

The results (solid lines in the lower three panels of Fig. 11) confirm that vertical wind at the mixed-layer depth varies seasonally and therefore contributes to the seasonal rectifier effect. Seasonal variability in the vertical wind at both SGP and LEF is such

ACPD
11, 11455–11495, 2011

that mixed-layer concentrations would be enhanced relative to the free-troposphere if the surface flux (F in Eq. 7) were seasonally varying but annually balanced, as in idealized modeling studies (Denning et al., 1995). Subsidence is strongest in winter at HFM, which may help to explain why vertical concentrations gradients at HFM are comparable to those at SGP and LEF, even though the net surface flux is significantly more positive there (c.f. panels Figs. 10, 9). The difference between vertical velocities at HFM and at the other two sites (SGP, LEF) can be explained by topographic forcing of flow over the Appalachian mountains (e.g. Saltzman and Irsch, 1972), which is strongest in winter due to stronger surface westerlies. According to Eq. (7), the coincidence of larger vertical wind with the strongest respiratory fluxes in winter helps to reduce winter mixed-layer concentrations relative to the free troposphere, bringing the winter vertical gradient at HFM closer to those of other sites.

The mechanism by which vertical transport contributes to the seasonal rectifier effect is clarified in height-time cross sections of the vertical wind field (Fig. 11, top three panels) with seasonal variability in mixed-layer depth overlaid (solid black lines in the top three panels of Fig. 11). Recall that only the downward vertical velocity is relevant to the vertical advective tendency of mixed-layer concentrations, since vertical transport out of the mixed-layer by itself has no effect on mixed-layer concentrations. Note that the 90 day average subsidence velocity at the 90 day average mixed layer depth (as indicated by the top three panels of Fig. 11) is not exactly the same as the 90 day average of daily subsidence velocity calculated at daily mixed layer depths (shown in the bottom three panels of Fig. 11 in solid black lines), but the differences are small. The monotonic increase in vertical velocity with height in the lowest 1–2 km is not surprising, since vertical velocity must vanish at the earth's surface in the absence of topography. More importantly, from Fig. 11 the seasonal rectifier effect depends on both the seasonal variation in mixed-layer depth and seasonal variation in subsidence rates.

The effect of deeper summer mixed layers is to mix concentrations exchanged at the earth's surface to a depth above that of the winter mixed layer, where transport by the

ACPD
11, 11455–11495, 2011

vertical and horizontal wind is correspondingly stronger. This effect can be seen in the lower three panels of Fig. 11, where the vertical wind at annually-averaged mixed-layer depths (dashed line) is compared to the wind at seasonally varying mixed-layer depths (solid line). This comparison indicates that seasonal variability in mixed-layer depth is essential to seasonal variability in transport at SGP and LEF, however the same comparison yields the opposite result at HFM, where mixed layer depth variations act to reduce seasonal variations in vertical transport. These results underscore the importance of considering seasonal variations in mixed layer depth and transport together when explaining vertical CO_2 gradients, and that mixed layer depth is not always a good indicator of the strength of mixing and transport.

5 Discussion

Boundary layer equilibrium has important consequences for the interpretation of CO_2 flux inversion errors. Given the surface flux, equilibrium predicts a simple inverse proportionality between CO_2 vertical gradients and the vertical wind ($\Delta c \approx -Fw^{-1}$, recalling that $\Delta c = c_m - c_f$), which is consistent with the hypothesis that weaker than observed summer vertical gradients resulted from overestimated vertical mixing in atmospheric models, while stronger than observed winter gradients resulted from underestimated mixing (Stephens et al., 2007). However it is also evident (from Eq. 7) that the inverse proportionality between errors in vertical gradients and mixing will only hold if there are no errors in the surface flux, horizontal advective transport, or non-linear vertical advective transport (i.e., synoptic-scale eddies). For example, systematic biases in vertical gradients could also result from the specification of the first-guess fluxes used in forward transport simulations prior to inversion, known as prior fluxes.

As a counter example to the hypothesis that vertical mixing is systematically biased in transport models, consider a hypothetical transport model simulation having perfect vertical mixing and transport but subject to specification of overestimated summer prior surface fluxes (shown schematically in Fig. 12). Accurate transport implies

ACPD
11, 11455–11495, 2011

that subsidence ($w < 0$) in this simulation always matches that of the real atmosphere. Overestimated summer fluxes (i.e., F less negative than observed) require larger free-tropospheric concentrations in the forward simulation (solid circles in Fig. 12a) than in observations (squares in Fig. 12a), and correspondingly weaker vertical gradients, according to $\Delta c \approx -Fw^{-1}$. Unless the inversion of this transport is tightly constrained to observed concentrations, the post-inversion vertical gradient may remain underestimated, falsely indicating summer overestimated mixing, while free-tropospheric concentrations would remain overestimated, falsely indicating underestimated summer mixing. This example illustrates why either CO_2 concentrations or vertical CO_2 gradients taken alone are not reliable indicators of transport model errors, and how opposite conclusions regarding CO_2 mixing can be drawn when free-troposphere concentrations are considered separately of mixed-layer concentrations.

Contradictory hypotheses of both summer overestimated and underestimated mixing could be reconciled if specified prior surface fluxes are overestimated, as discussed above, without having to invoke systematic transport model biases. Possible overestimation of prior summer fluxes has been suggested as a result of seasonality in fossil fuel emissions (Gurney et al., 2005; Erickson et al., 2008) or underestimated seasonal amplitudes of specified prior biospheric fluxes (Peters et al., 2007; Yang et al., 2007), which have not been considered in past analyses of CO_2 inversion sensitivity to transport. Previous studies using SF_6, an ideal tracer due to its well known and seasonally invariant emissions, found no systematic errors in summer modeled transport (Gloor et al., 2007; Patra et al., 2009). Overestimated prior fluxes would enhance predicted boundary-layer CO_2 concentrations relative to the free-troposphere in forward transport model simulations (Fig. 12a), requiring compensating stronger summer biospheric uptake in the inversions when constrained by observed concentrations Gurney et al., 2005). This process could explain why the northern land sink is larger in inverse estimates than carbon inventories.

The possibility of underestimated summer mixing (Yang et al., 2007) should be examined carefully, because erroneously weak vertical mixing, if it exists and is corrected

ACPD
11, 11455–11495, 2011

in transport models, could increase the discrepancy between inversion estimates and land carbon inventories. Increased mixing rates (more negative w) would result in stronger modeled vertical gradients relative to observations (Δc more negative in $\Delta c \approx -F w^{-1}$), requiring an even larger land carbon sink in the inversions. The process is shown schematically in Fig. 12c (circles and squares indicate model and observations, respectively) and contrasted with that of overestimated summer mixing (Fig. 12b). In the case of overestimated summer mixing, the hypothetical perfect prior flux would be adjusted to take up more CO_2 in order to minimize differences between the forward-transport simulation and observations in the inversion procedure. Overestimated summer mixing would therefore be more desirable with regard to explaining why the land carbon sink is stronger in inversion estimates than in land carbon inventories.

Underestimated model mixed layer depths (Yi et al., 2004; Denning et al., 2008) have been cited as a mechanism for underestimated summer mixing, and as an explanation for underestimated seasonal amplitudes of modeled free-tropospheric and column-average CO_2 (Yang et al., 2007), presumably due to dilution and transient entrainment associated with the growth of deep mixed-layers. However the direct effect of mixed layer depths on the dilution of concentrations is an order of magnitude smaller than transport at seasonal timescales (see Sect. 2.2). We therefore consider the indirect effect of mixed layer depths through the dependence of subsidence rates on depth above the surface. Seasonality in mixed layer depth can oppose seasonality in the vertical gradient of subsidence, for example at HFM, a site exhibiting the same biases in modeled vertical CO_2 gradients as other sites (Stephens et al., 2007). Seasonality in mixing strength is reversed at HFM relative to other sites even though the seasonality in mixed-layer depth is not. Mixed-layer depth is therefore a poor indicator of mixing rates. It is necessary to consider both the divergent wind field and the mixed-layer depth together when assessing transport model performance.

We have not considered convective cloud mass fluxes, and so may underestimate the extent to which spring and summer flux inversions could be in error due to transport model errors. However, the resolved-scale subsidence velocity in the data assimilation

ACPD
11, 11455–11495, 2011

systems used here is required to reflect the aggregate effects of transport and mixing at the sub-grid scale, due to separate enforcement of mass and energy balance at both sub-grid and global scales in the models underlying these datasets (Lawrence and Salzmann, 2008). This process is reflected in the reasonable agreement between surface fluxes and vertical gradients from data assimilation systems and those reconstructed using the equilibrium approximation and resolved-scale model winds. Improvements to the parameterization of mixing and transport by convective clouds are still needed, especially since these parameterizations were designed to realistically simulate energy balances for climate studies rather than tracer transport.

General circulation models have a well-known bias in the diurnal timing of deep convection (e.g. Guichard et al., 2004), with a preference toward local noon, whereas observed continental convection has a preference for the evening and nighttime (e.g. Wallace, 1975). Enhanced deep-convection during peak respiration would tend to reduce near-surface CO_2 concentrations relative to the free troposphere, enhancing the summer depletion of mixed-layer CO_2 relative to the free-troposphere. This process could explain why summer near-surface CO_2 is more depleted in observations than transport models despite apparent lack of similar biases in other trace gases, such as SF_6 (Gloor et al., 2007).

6 Conclusions

Previous hypotheses for transport model errors assumed that boundary layer depth and vertical CO_2 gradients reflect the strength of vertical mixing in the lower-troposphere. However seasonality in the strength of transport and mixing is anti-correlated with boundary layer depth at some sites, diminishing in summer when the boundary layer is deepest. Vertical CO_2 gradients are also unreliable indicators of mixing because surface fluxes and mixing both contribute to vertical concentration gradients.

We developed a new diagnostic model to understand vertical CO_2 gradients and their relation to atmospheric transport and mixing, based on the concept of boundary layer

ACPD
11, 11455–11495, 2011

equilibrium, and demonstrated its application to long-term observations and a global data assimilation system. The finite timescale over which observed concentration gradients relax toward equilibrium is diagnostic of the rate at which boundary layer air is exchanged with the free-troposphere. This diagnostic does not depend on model variables such as vertical velocity and is independent of seasonal surface fluxes.

Boundary layer equilibrium is an idealized concept that cannot account for the full complexity of atmospheric transport and mixing. Yet even in terms of this simplified description, many observations cited as evidence for systematic biases in atmospheric transport models are insufficient to prove that such biases exist, and in some cases model errors proposed to reconcile carbon inventory and inverse estimates of global carbon sinks could confound these estimates. Atmospheric transport model errors are widely cited as contributing to uncertainty in CO_2 flux inversions, but the problem of identifying or refuting these errors remains. The methods developed here can be used to diagnose the several factors leading to uncertainty in global inversions of surface CO_2 fluxes.

Acknowledgement. Funding for this study was provided by the US Department of Energy, BER Program, Contract # DE-AC02-05CH11231. CarbonTracker 2008 results provided by NOAA ESRL, Boulder, Colorado, USA from the website at carbontracker.noaa.gov. Andy Jacobson assisted with the CarbonTracker data.

References

Baker, D. F., Law, R. M., Gurney, K. R., Rayner, P., Peylin, P., Denning, A. S., Bousquet, P., Bruhwiler, L., Chen, Y. H., Ciais, P., Fung, I. Y., Heimann, M., John, J., Maki, T., Maksyutov, S., Masarie, K., Prather, M., Pak, B., Taguchi, S., and Zhu, Z.: TransCom 3 inversion intercomparison: impact of transport model errors on the interannual variability of regional CO_2 fluxes, 1988–2003, Global Biogeochem. Cy., 20, doi:10.1029/2004GB002439, 2006. 11457

Bakwin, P. S., Tans, P. P., Zhao, C. L., Ussler, W., and Quesnell, E.: Measurements of carbon-dioxide on a very tall tower, Tellus B, 47, 535–549, 1995. 11461

ACPD

11, 11455–11495, 2011

Bakwin, P. S., Davis, K. J., Yi, C., Wofsy, S. C., Munger, J. W., Haszpra, L., and Barcza, Z.: Regional carbon dioxide fluxes from mixing ratio data, Tellus B, 56, 301–311, 2004. 11460, 11466

Bousquet, P., Peylin, P., Ciais, P., Le Quere, C., Friedlingstein, P., and Tans, P. P.: Regional changes in carbon dioxide fluxes of land and oceans since 1980, Science, 290, 1342–1346, 2000. 11457

Chatfield, C.: The Analysis of Time Series, Chapman & Hall, New York, USA, 2004. 11468

Chen, B. Z., Chen, J. M., Liu, J., Chan, D., Higuchi, K., and Shashkov, A.: A vertical diffusion scheme to estimate the atmospheric rectifier effect, J. Geophys. Res.-Atmos., D04306, doi:10.1029/2003JD003925, 109, 2004. 11457

Chou, W. W., Wofsy, S. C., Harriss, R. C., Lin, J. C., Gerbig, C., and Sachse, G. W.: Net fluxes of CO_2 in Amazonia derived from aircraft observations, J. Geophys. Res.-Atmos., 107, D04614, doi:10.1029/2001JD001295, 2002. 11460

Conway, T. J., Tans, P. P., Waterman, L. S., and Thoning, K. W.: Evidence for interannual variability of the carbon-cycle from the National Oceanic and Atmospheric Administration Climate Monitoring and Diagnostics Laboratory Global Air-Sampling Network, J. Geophys. Res.-Atmos., 99, 22831–22855, 1994. 11461

Cooley, H. S., Riley, W. J., Torn, M. S., and He, Y.: Impact of agricultural practice on regional climate in a coupled land surface mesoscale model, J. Geophys. Res.-Atmos., 110, D03113, doi:10.1029/2004jd005160, 2005. 11461

Dargaville, R. J., Doney, S. C., and Fung, I. Y.: Inter-annual variability in the interhemispheric atmospheric CO_2 gradient: contributions from transport and the seasonal rectifier, Tellus B, 55, 711–722, 2003. 11457

Davis, K. J., Bakwin, P. S., Yi, C. X., Berger, B. W., Zhao, C. L., Teclaw, R. M., and Isebrands, J. G.: The annual cycles of CO_2 and H_2O exchange over a northern mixed forest as observed from a very tall tower, Glob. Change Biol., 9, 1278–1293, 2003. 11462

Denman, K. L., Brasseur, G., Chidthaisong, A., Ciais, P., Cox, P. M., Dickinson, R. E., Hauglustaine, D., Heinze, C., Holland, E., Jacob, D., Lohmann, U., Ramachandran, S., da Silva Dias, P. L., Wofsy, S. C., and Zhang, X., Couplings between changes in the climate system and biogeochemistry, in: Climate change 2007: The physical science basis. Contribution of working group I to the fourth assessment report of the intergovernmental panel on climate change, edited by: Solomon, S., Qin, D., Manning, M., Chen, Z., Marquis, M., Averyt, K. B., Tignor, M., and Miller, H. L., Cambridge University Press, Cambridge, New York, USA, 2007.

ACPD
11, 11455–11495, 2011

11456
Denning, A. S., Fung, I. Y., and Randall, D.: Latitudinal gradient of atmospheric CO_2 due to seasonal exchange with land biota, Nature, 376, 240–243, 1995. 11457, 11473
Denning, A. S., Holzer, M., Gurney, K. R., Heimann, M., Law, R. M., Rayner, P. J., Fung, I. Y., Fan, S. M., Taguchi, S., Friedlingstein, P., Balkanski, Y., Taylor, J., Maiss, M., and Levin, I.: Three-dimensional transport and concentration of SF6 – a model intercomparison study (TransCom 2), Tellus B, 51, 266–297, 1999. 11470
Denning, A. S., Zhang, N., Yi, C. X., Branson, M., Davis, K., Kleist, J., and Bakwin, P.: Evaluation of modeled atmospheric boundary layer depth at the WLEF tower, Agr. Forest Meteor., 148, 206–215, 2008. 11457, 11476
Emanuel, K.: Atmospheric Convection, Oxford University Press, New York, USA, 1994. 11458
Erickson, D. J., Mills, R. T., Gregg, J., Blasing, T. J., Hoffman, F. M., Andres, R. J., Devries, M., Zhu, Z., and Kawa, S. R.: An estimate of monthly global emissions of anthropogenic CO_2: Impact on the seasonal cycle of atmospheric CO_2, J. Geophys. Res.-Biogeo., 113, G01023, doi:10.1029/2007jg000435, 2008. 11475
Fischer, M. L., Billesbach, D. P., Berry, J. A., Riley, W. J., and Torn, M. S.: Spatiotemporal variations in growing season exchanges of CO_2, H_2O, and sensible heat in agricultural fields of the Southern Great Plains, Earth Interact., 11(17), 1–21, 2007. 11461
Friedlingstein, P., Cox, P., Betts, R., Bopp, L., Von Bloh, W., Brovkin, V., Cadule, P., Doney, S., Eby, M., Fung, I., Bala, G., John, J., Jones, C., Joos, F., Kato, T., Kawamiya, M., Knorr, W., Lindsay, K., Matthews, H. D., Raddatz, T., Rayner, P., Reick, C., Roeckner, E., Schnitzler, K. G., Schnur, R., Strassmann, K., Weaver, A. J., Yoshikawa, C., and Zeng, N.: Climate-carbon cycle feedback analysis: results from the (CMIP)-M-4 model intercomparison, J. Climate, 19, 3337–3353, 2006. 11456
Fung, I., Prentice, K., Matthews, E., Lerner, J., and Russell, G.: 3-dimensional tracer model study of atmospheric CO_2 – response to seasonal exchanges with the terrestrial biosphere, J. Geophys. Res.-Oc. Atm., 88, 1281–1294, 1983. 11457
Gloor, M., Fan, S. M., Pacala, S., Sarmiento, J., and Ramonet, M.: A model-based evaluation of inversions of atmospheric transport, using annual mean mixing ratios, as a tool to monitor fluxes of nonreactive trace substances like CO_2 on a continental scale, J. Geophys. Res.-Atmos., 104, 14245–14260, 1999. 11457
Gloor, M., Dlugokencky, E., Brenninkmeijer, C., Horowitz, L., Hurst, D. F., Dutton, G., Crevoisier, C., Machida, T., and Tans, P.: Three-dimensional SF6 data and tropospheric

ACPD
11, 11455–11495, 2011

transport simulations: signals, modeling accuracy, and implications for inverse modeling, J. Geophys. Res.-Atmos., 110, D10308, doi:10.1029/2004jd005373, 2007. 11475, 11477

Guichard, F., Petch, J. C., Redelsperger, J. L., Bechtold, P., Chaboureau, J. P., Cheinet, S., Grabowski, W., Grenier, H., Jones, C. G., Kohler, M., Piriou, J. M., Tailleux, R., and Tomasini, M.: Modelling the diurnal cycle of deep precipitating convection over land with cloud-resolving models and single-column models, Q. J. Roy. Meteor. Soc., 130, 3139–3172, 2004. 11477

Gurney, K. R., Chen, Y. H., Maki, T., Kawa, S. R., Andrews, A., and Zhu, Z. X.: Sensitivity of atmospheric CO_2 inversions to seasonal and interannual variations in fossil fuel emissions, J. Geophys. Res.-Atmos., 110, D10308, doi:10.1029/2004jd005373, 2005. 11475

Helliker, B. R., Berry, J. A., Betts, A. K., Bakwin, P. S., Davis, K. J., Denning, A. S., Ehleringer, J. R., Miller, J. B., Butler, M. P., and Ricciuto, D. M.: Estimates of net CO_2 flux by application of equilibrium boundary layer concepts to CO_2 and water vapor measurements from a tall tower, J. Geophys. Res.-Atmos., 109, D20106, doi:10.1029/2004JD004532, 2004. 11460, 11466

Lawrence, M. G. and Salzmann, M.: On interpreting studies of tracer transport by deep cumulus convection and its effects on atmospheric chemistry, Atmos. Chem. Phys., 8, 6037–6050, doi:10.5194/acp-8-6037-2008, 2008. 11477

Levy, P. E., Grelle, A., Lindroth, A., Molder, M., Jarvis, P. G., Kruijt, B., and Moncrieff, J. B.: Regional-scale CO_2 fluxes over Central Sweden by a boundary layer budget method, Agr. Forest Meteor., 98–9, 169–180, 1999. 11457

Lloyd, J., Francey, R. J., Mollicone, D., Raupach, M. R., Sogachev, A., Arneth, A., Byers, J. N., Kelliher, F. M., Rebmann, C., Valentini, R., Wong, S. C., Bauer, G., and Schulze, E. D.: Vertical profiles, boundary layer budgets, and regional flux estimates for CO_2 and its $^{13}C/^{12}C$ ratio and for water vapor above a forest/bog mosaic in Central Siberia, Global Biogeochem. Cy., 15, 267–284, 2001. 11457

North, G. R., Bell, R. E., and Hardin, J. W.: Fluctuation dissipation in a general circulation model, Clim. Dynam., 8, 259–264, 1993. 11468

Patra, P. K., Takigawa, M., Dutton, G. S., Uhse, K., Ishijima, K., Lintner, B. R., Miyazaki, K., and Elkins, J. W.: Transport mechanisms for synoptic, seasonal and interannual SF_6 variations and "age" of air in troposphere, Atmos. Chem. Phys., 9, 1209–1225, doi:10.5194/acp-9-1209-2009, 2009. 11475

Peters, W., Jacobson, A. R., Sweeney, C., Andrews, A. E., Conway, T. J., Masarie, K.,

ACPD
11, 11455–11495, 2011

Miller, J. B., Bruhwiler, L. M. P., Petron, G., Hirsch, A. I., Worthy, D. E. J., van der Werf, G. R., Randerson, J. T., Wennberg, P. O., Krol, M. C., and Tans, P. P.: An atmospheric perspective on North American carbon dioxide exchange: CarbonTracker, P. Natl. Acad. Sci. USA, 104, 18925–18930, 2007. 11462, 11475

Peylin, P., Baker, D., Sarmiento, J., Ciais, P., and Bousquet, P.: Influence of transport uncertainty on annual mean and seasonal inversions of atmospheric CO_2 data, J. Geophys. Res.-Atmos., 107(D19), 4385, doi:10.1029/2001JD000857, 2002. 11457

Raupach, M. R.: Vegetation-atmosphere interaction in homogeneous and heterogeneous terrain – some implications of mixed-layer dynamics, Vegetatio, 91, 105–120, 1991. 11457

Raupach, M. R., Denmead, O. T., and Dunin, F. X.: Challenges in linking atmospheric CO_2 concentrations to fluxes at local and regional scales, Aust. J. Bot., 40, 697–716, 1992. 11457

Raymond, D. J.: Boundary layer quasi-equilibrium (BLQ), in: The Physics and Parameterization of Moist Convection, edited by: Smith, R. K., Kluwer Academic Publishers, Dordrecht, The Netherlands, 1997. 11467

Riley, W. J., Biraud, S. C., Torn, M. S., Fischer, M. L., Billesbach, D. P., and Berry, J. A.: Regional CO_2 and latent heat surface fluxes in the Southern Great Plains: measurements, modeling, and scaling, J. Geophys. Res.-Biogeo., 114, G04009, doi:10.1029/2009JG001003, 2009. 11461

Rödenbeck, C., Houweling, S., Gloor, M., and Heimann, M.: CO_2 flux history 1982–2001 inferred from atmospheric data using a global inversion of atmospheric transport, Atmos. Chem. Phys., 3, 1919–1964, doi:10.5194/acp-3-1919-2003, 2003. 11457

Saltzman, B. and Irsch, F. E.: Note on the theory of topographically forced planetary waves in atmosphere, Mon. Weather Rev., 100, 441–444, 1972. 11473

Stephens, B. B., Gurney, K. R., Tans, P. P., Sweeney, C., Peters, W., Bruhwiler, L., Ciais, P., Ramonet, M., Bousquet, P., Nakazawa, T., Aoki, S., Machida, T., Inoue, G., Vinnichenko, N., Lloyd, J., Jordan, A., Heimann, M., Shibistova, O., Langenfelds, R. L., Steele, L. P., Francey, R. J., and Denning, A. S.: Weak northern and strong tropical land carbon uptake from vertical profiles of atmospheric CO_2, Science, 316, 1732–1735, 2007. 11457, 11458, 11463, 11464, 11474, 11476

Styles, J. M., Lloyd, J., Zolotoukhine, D., Lawton, K. A., Tchebakova, N., Francey, R. J., Arneth, A., Salamakho, D., Kolle, O., and Schulze, E. D.: Estimates of regional surface carbon dioxide exchange and carbon and oxygen isotope discrimination during photosynthesis from concentration profiles in the atmospheric boundary layer, Tellus B, 54, 768–783, 2002. 11457

ACPD
11, 11455–11495, 2011

Wallace, J. M.: Diurnal-variations in precipitation and thunderstorm frequency over conterminous United-States, Mon. Weather Rev., 103, 406–419, 1975. 11477

Yang, Z., Washenfelder, R. A., Keppel-Aleks, G., Krakauer, N. Y., Randerson, J. T., Tans, P. P., Sweeney, C., and Wennberg, P. O.: New constraints on Northern Hemisphere growing season net flux, Geophys. Res. Lett., 34, L12807, doi:10.1029/2007GL029742, 2007. 11457, 11475, 11476

Yi, C., Davis, K. J., Bakwin, P. S., Denning, A. S., Zhang, N., Desai, A., Lin, J. C., and Gerbig, C.: Observed covariance between ecosystem carbon exchange and atmospheric boundary layer dynamics at a site in Northern Wisconsin, J. Geophys. Res.-Atmos., D08302, doi:10.1029/2003JD004164, 109, 2004. 11457, 11460, 11476

Yi, C. X., Davis, K. J., Berger, B. W., and Bakwin, P. S.: Long-term observations of the dynamics of the continental planetary boundary layer, J. Atmos. Sci., 58, 1288–1299, 2001. 11459

ACPD

11, 11455–11495, 2011

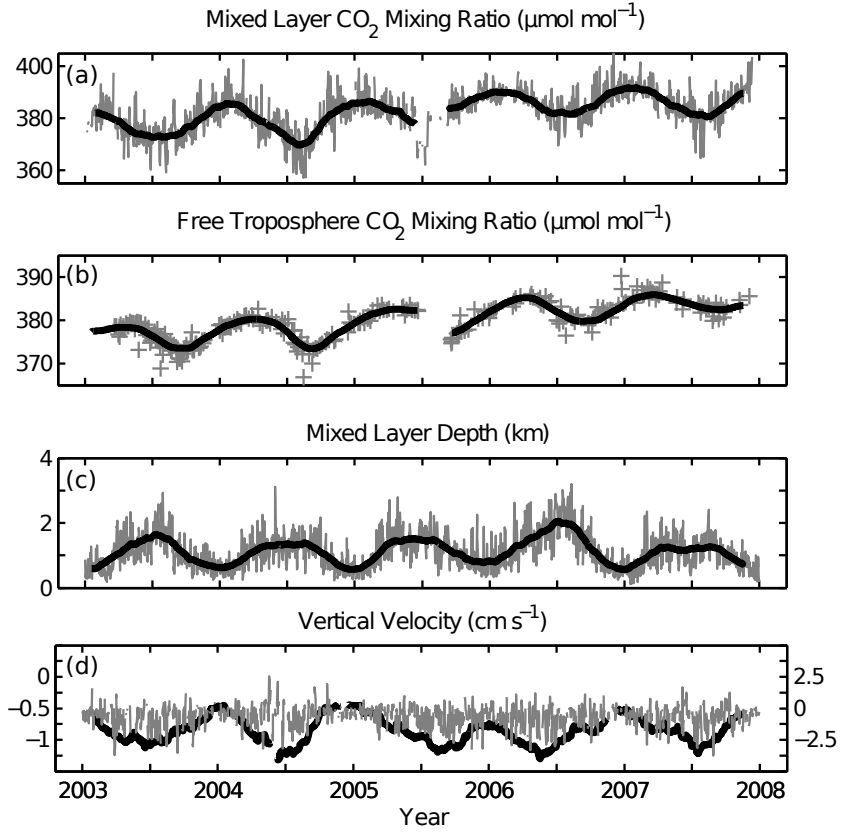

Fig. 1. Timeseries at SGP: CO_2 mixing ratios from 60 m tower **(a)** and from aircraft flask samples above the mixed layer **(b)**, mixed layer depth from CT/TM5 model output **(c)**, and vertical velocity from ECMWF interim reanalysis **(d)**. Daily averages, 90 day averages, and instantaneous values are indicated by gray lines, thick black lines, and crossbars (+), respectively. The left and right axes of **(d)** correspond to the 90 day subsidence and daily vertical velocity averages, respectively

ACPD
11, 11455–11495, 2011

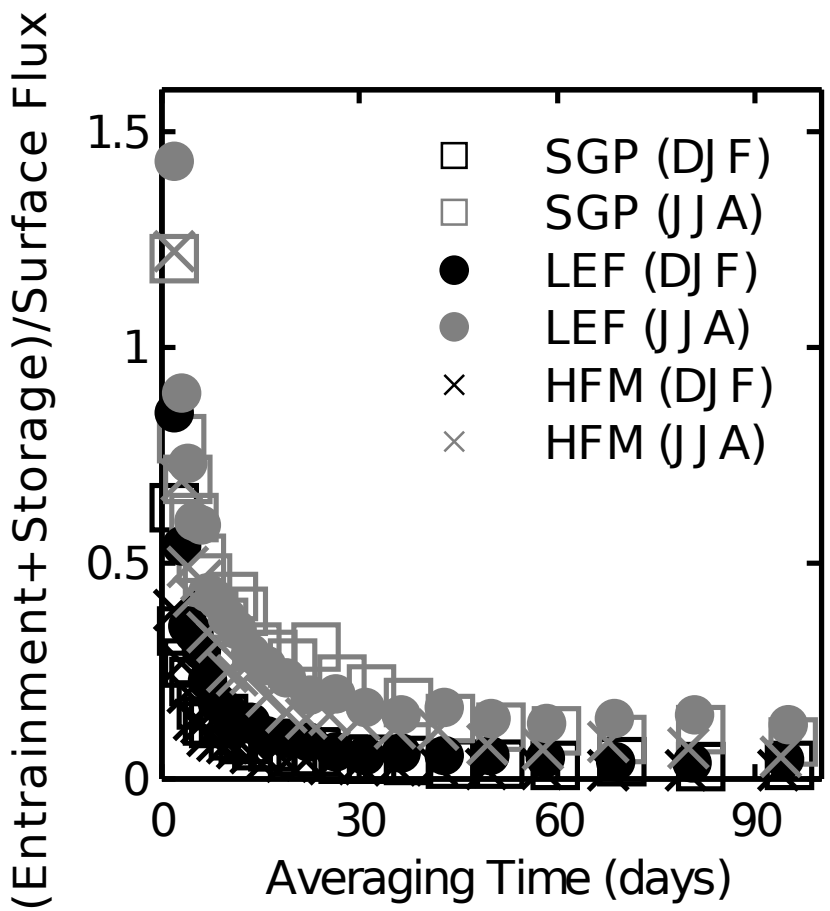

Fig. 2. Ratios of the sum of entrainment and storage to net surface flux, for various averaging times between 1 and 90 days during June–August (JJA) and December–February (DJF). Ratios were calculated from the CT model output combined with meteorological data from ECMWF (see text for details).

ACPD
11, 11455–11495, 2011

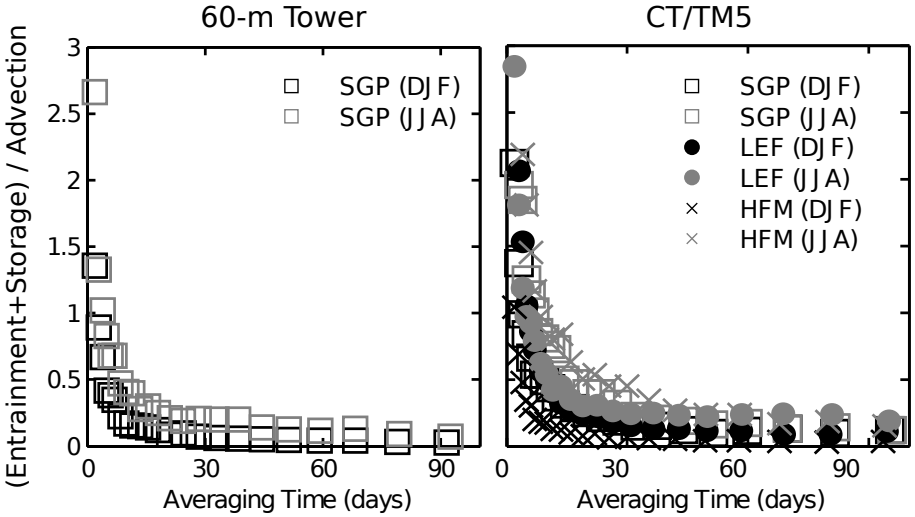

Fig. 3. As in Fig. 2 but for the ratio of the sum of entrainment and storage to vertical advection calculated from 60 m tower and aircraft observations at SGP **(a)** and from CT/TM5 at SGP, LEF, and HFM **(b)**.

ACPD
11, 11455–11495, 2011

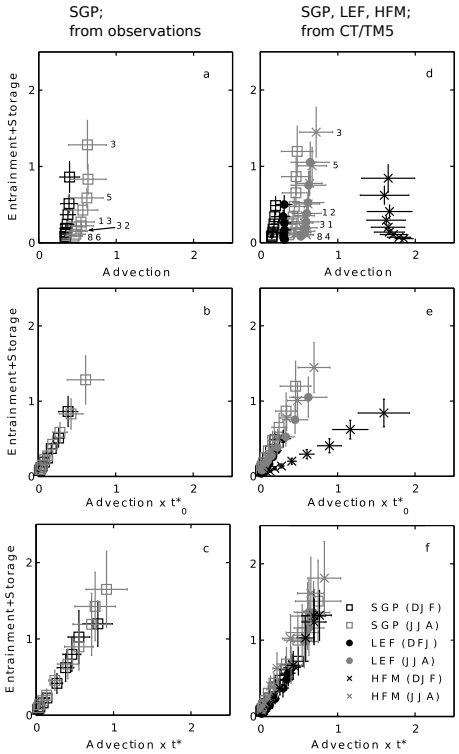

Fig. 4. Magnitudes of entrainment and storage (summed), and vertical advection (in $\mu mol\,m^{-2}\,s^{-1}$), based on observations at SGP **(a–c)**, and on CT model output at SGP, LEF, and HFM **(d–f)**. Values of entrainment, storage, and vertical advection, were binned according to the averaging time **(a, d)** or the nondimenisonal numbers $t_0^* = H_0/W_0T$ **(b, e)** and $t^* = H/WT$ **(c, f)** (see text for definitions). Averaging was performed over each bin (width of cross bars gives half the standard deviation) and vertical advection was scaled according to each bin value in panels **(b, c, e, f)**. For illustration, a few representative averaging times are indicated in panels **(a, d)** for SGP and HFM for June–August (see text for details).

ACPD
11, 11455–11495, 2011

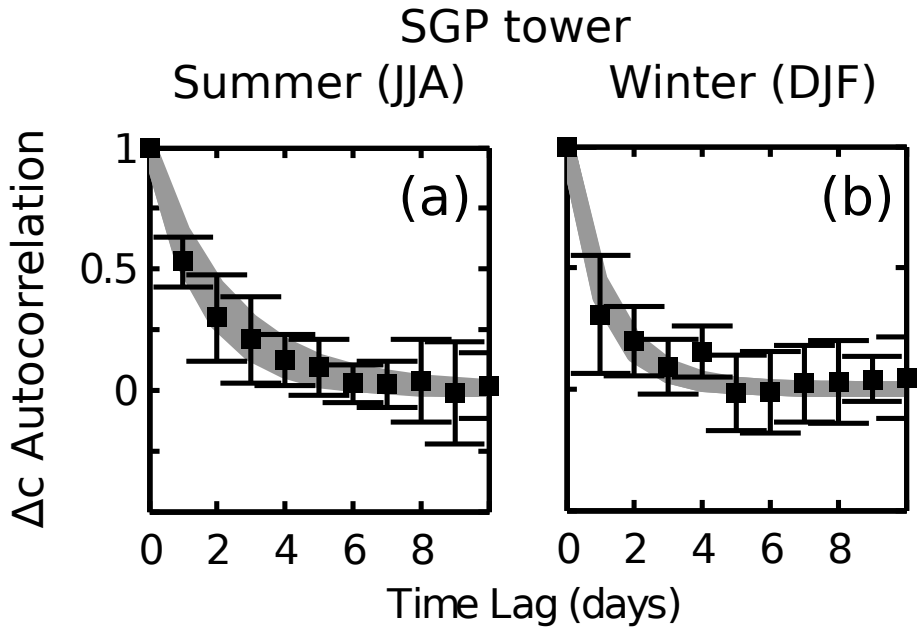

Fig. 5. Autocorrelation coefficient for perturbations in daily vertical mixing ratio gradients from 90 day running averages at SGP (using aircraft and 60 m tower observations), calculated for each year between 2003 and 2007 separately before averaging over all years. Error bars indicate the standard deviation of the mean over all years. Panels **(a)** and **(b)** correspond to summer and winter, respectively. The gray line indicates exponential decay toward the 90 day average value with rate constant t^* (see text for details).

ACPD
11, 11455–11495, 2011

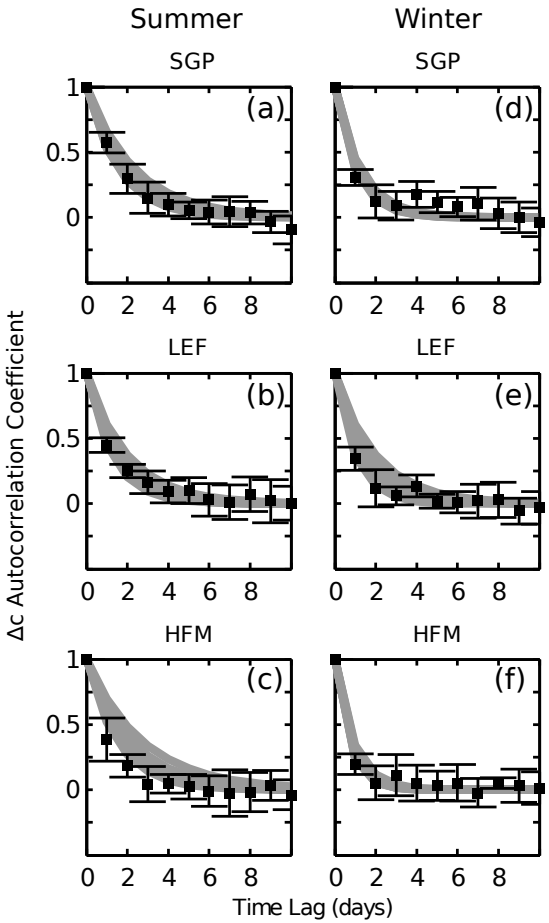

Fig. 6. As in Fig. 5 but using vertical mixing ratio gradients from the CT model during summer at SGP **(a)**, LEF **(b)**, and HFM **(c)**, and winter **(d–f)**.

ACPD
11, 11455–11495, 2011

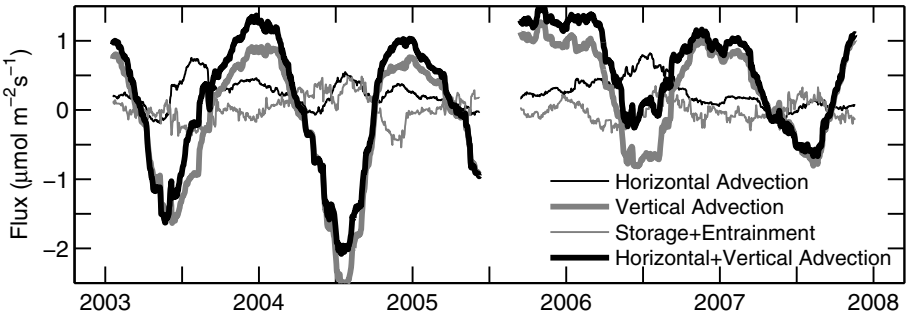

Fig. 7. Contribution of mixed-layer budget terms to the surface flux at SGP, calculated from 90 day running averages using 60 m tower and aircraft mixing ratios, and decomposed into horizontal advection (thin black), vertical advection (thick gray), storage plus entrainment (thin gray) and horizontal plus vertical advection (thick black).

ACPD
11, 11455–11495, 2011

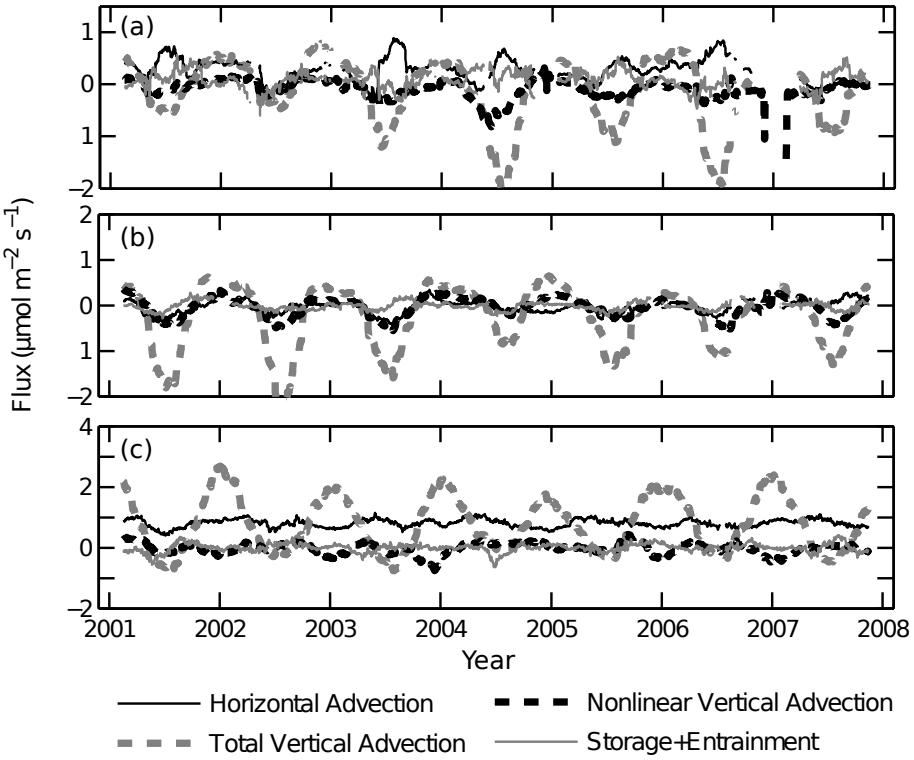

Fig. 8. Contribution of mixed-layer budget terms to the net surface CO_2 flux calculated from CT/TM5 assimilated concentrations at SGP **(a)**, LEF **(b)**, and HFM **(c)**.

ACPD
11, 11455–11495, 2011

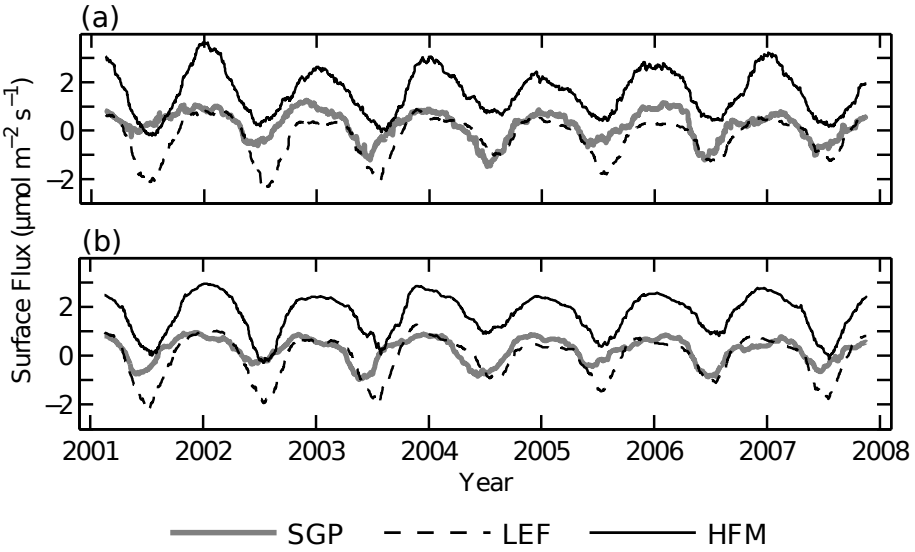

Fig. 9. Surface flux inferred from the equilibrium approximation **(a)** and the CT/TM5 assimilated surface flux **(b)** for SGP (gray), LEF (dashed), and HFM (solid), using 90 day averages. Equilibrium fluxes are given by the sum of horizontal and total vertical advection shown in Fig. 8.

ACPD
11, 11455–11495, 2011

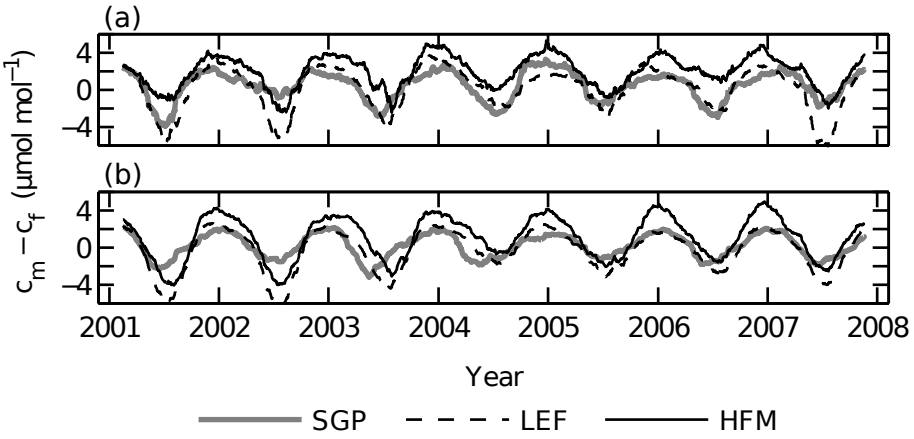

Fig. 10. Vertical mixing ratio gradient inferred from the equilibrium approximation **(a)** and from the CT/TM5 data assimilation system **(b)** at SGP (gray), LEF (dashed), and HFM (solid), using 90 day averages.

ACPD
11, 11455–11495, 2011

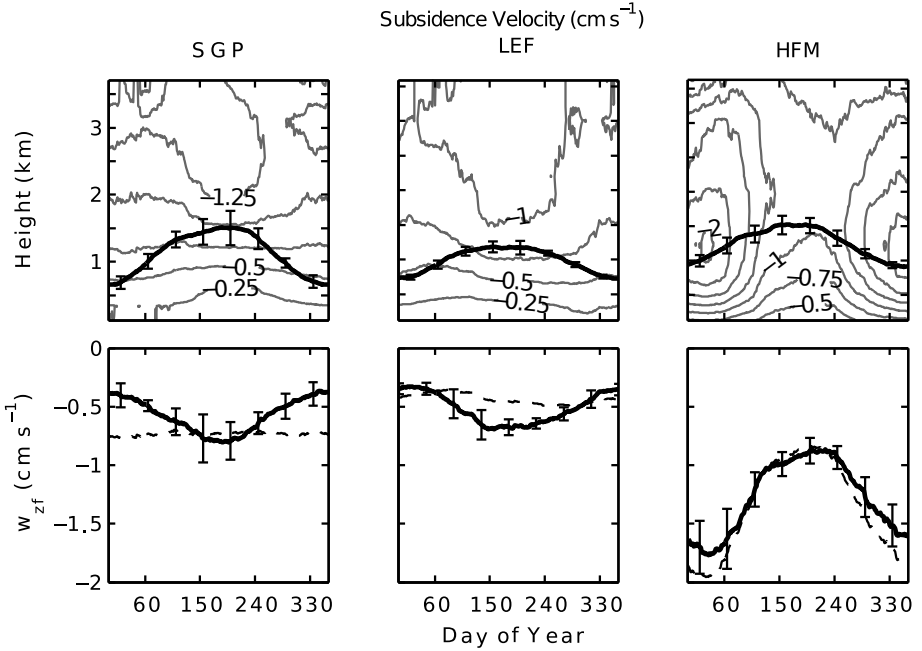

Fig. 11. Top: mean annual cycle of subsidence velocity (where $w < 0$) calculated from ECMWF data (years 2001–2007), contoured every 0.25 cm s^{-1}, overlaid with CT/TM5 90 day running average maximum daily mixed layer height (error bars indicate standard deviation of the mean). Below: subsidence velocity at the 90 day running average mixed layer top (w_{zf}) (solid line) and at the annual average (constant) mixed layer depth (dashed line).

ACPD
11, 11455–11495, 2011

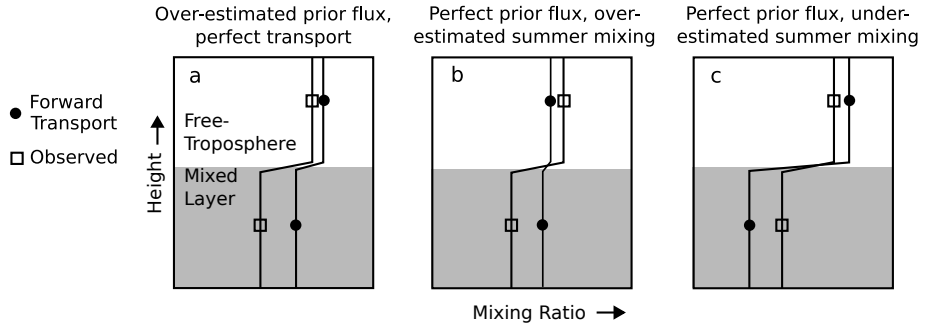

Fig. 12. Panel **(a)**: schematic illustrating a hypothetical perfect summer transport model simulation (solid circles) forced with either summer overestimated continental mixed-layer concentrations or overestimated prior surface flux, and the observed free-troposphere and mixed layer concentrations (squares). Panel **(b)**: as in **(a)** but for a hypothetical transport model simulation having correctly specified prior surface fluxes but overestimated vertical mixing. Panel **(c)**: as in **(b)** but for underestimated vertical mixing. The mixed layer is indicated in gray shading.

ACPD
11, 11455–11495, 2011